Electronic structure of random binary alloys

1996 J. Phys.: Condens. Matter 8 1979

(http://iopscience.iop.org/0953-8984/8/12/012)

J. Phys.: Condens. Matter **8** (1996) 1979–1996. Printed in the UK

Electronic structure of random binary alloys

Tanusri Saha, Indra Dasgupta† and Abhijit Mookerjee

S N Bose National Centre for Basic Sciences, DB 17, Sector 1, Salt Lake City, Calcutta 700064, India

Received 15 May 1995

Abstract. We present here an application of the augmented-space recursion technique for binary disordered alloys. The method allows us to incorporate effects like clustering, short-ranged order and off-diagonal disorder arising out of size mismatch and consequent lattice distortions. We base our calculations on the TB-LMTO Hamiltonian of Andersen and co-workers. We study three alloy systems: AgPd, CuZn and FeTi, and compare our results with earlier work.

1. Introduction

The first-principles description of the electronic structure and properties of disordered transition metal alloys is a challenging problem. The absence of translational symmetry is the main obstacle in the construction of a quantitative theory comparable in accuracy and efficiency with those for crystalline solids, based on the Bloch theorem and standard band-structure methods. The electronic structure and properties of transition metal alloys are believed to be governed mainly by the relatively localized d electrons. Hence it was customary to use semi-empirical tight-binding Hamiltonians to describe their electronic properties. In spite of encouraging successes, the electronic structure calculations based on semi-empirical tight-binding Hamiltonians have some underlying approximations which are often unjustified [1].

The main step towards constructing first-principles tight-binding Hamiltonians began with the tight-binding linearized muffin-tin orbital (TB-LMTO) method proposed by Andersen and Jepsen [2]. In the TB-LMTO method the Hamiltonian is parametrized with a set of potential parameters (to be discussed later in the text) which are derived self-consistently from a first-principles theory and are not empirical.

The other central issue for a first-principles calculation is the construction of realistic structural models. In principle, the structure can be varied in parallel to the calculation of electronic structure. This has been reformulated in terms of classical Lagrangian dynamics by Car and Parinello [3]. This method has been extensively used in *ab initio* molecular dynamics simulations of liquid and amorphous Si and other s–p-bonded systems, but the underlying pseudopotential method makes its application to systems with transition metals impractical. Recently there have been attempts at *ab initio* molecular dynamics studies based on the full-potential LMTO method. Methfessel and Schilfgaarde [4] have derived an accurate force theorem, quite distinct from the Hellmann–Feynman theorem. They have implemented a Car–Parinello type of dynamics in a new full-potential LMTO method,

† Present address: Max-Planck-Institut für Festkörperforschung, D-70569, Stuttgart, Germany.

0953-8984/96/121979+18$19.50

which is suitable for arbitrary geometries, and calculated the properties of small Ag clusters. Though first-principles electronic structure calculations for topologically disordered systems demand realistic structural models, for substitutionally disordered transition metal alloys calculations in the TB-LMTO framework are regarded to be first-principles ones.

Kudrnovský and Drchal [5] have demonstrated that the coherent potential approximation (CPA) based on the linearized version of the screened KKR model (the TB-LMTO method) accurately describes the electronic structure of random alloys (both metallic and semiconducting) and disordered surfaces for a large class of alloy systems. Within the TB-LMTO method full charge self-consistency can be achieved and is usually used for elements, compounds and ordered alloys. Kudrnovský *et al* [6] have demonstrated that the flexibility in the choice of Wigner–Seitz radii in random binary alloys makes possible approximate, yet accurate and consistent, treatment of charge self-consistency without going through the full charge self-consistency cycle. The self-consistency involved in the solution of the CPA equation is not trivial and one has to invoke subtle mathematical procedures to ensure proper convergence. Recently Singh and Gonis [7] have criticized the TB-LMTO-CPA proposed by Kudrnovský and Drchal on the grounds that the ensemble or configuration averaging involved in their method did not properly take into account the multisite nature of the TB-LMTO basis functions, resulting in an inconsistency in the configuration-averaged Green function. Although these authors try to circumvent this difficulty by making a pure L-approximation for the site-diagonal LMTOs, the fact remains that, by its very nature, the TB-LMTO formalism involves multisite summations.

Formally the APW [8] and the KKR methods [9], the 'parents' of the LAPW [10] and the LMTO methods [11] respectively, involve very few uncontrolled approximations and are therefore expected to be superior in accuracy and reliability to their linearized variants. However, solving the non-linear secular equations involved is computationally costly. Extensions of these methods to disordered systems further emphasize the computational difficulties. Of the mean-field approaches, the single-site CPA has been successfully implemented within these frameworks [12]. Certainly, where the single-site approximation is valid, the APW and KKR-CPA methods are the most accurate and reliable ones. However, there are many situations where such single-site approximations begin to fail—such as in cases where clustering effects become important [13] (e.g., in the impurity bands of split-band alloys, like the Zn band in Cu-rich CuZn alloys), where short-range order dominates leading to ordering or segregation [14], where local lattice distortions arising because of size mismatch of the constituents lead to essential off-diagonal disorder in the structure matrix $S_{RL,R'L'}$ [15] (as in CuPd or CuBe alloys), and where topological disorder of the underlying lattice makes the structure matrix depend on the specific pair of sites $\{R, R'\}$ [16] (such as in glassy materials like FeB). In such situations, the generalization of the CPA is not a trivial problem [13]. The embedded-cluster method (ECM) [17] where a cluster, in all its various disordered configurations, is embedded in a CPA medium, is not self-consistent in the spirit of CPAs. The molecular CPA [18] breaks the translational symmetry of the averaged medium, and the artificial zone-boundary effects introduced cannot be controlled. Of the cluster generalizations, only two retain *herglotz* analytic properties: the travelling-cluster approximation (TCA) [19] and the cluster CPA (CCPA) [20], both based on the augmented-space formalism (ASF) [21], which is also the basis of the work presented here. The computational intractability of both these methods whenever the size of the cluster becomes even reasonably large is clearly perceived by reference to [19, 20]. To date, calculations using the KKR-based CCPA have been successfully carried out only on pair clusters [22].

This provides a motivation for looking for alternative approaches for the generalization

of the single-site approximation. The TB-LMTO method is a likely framework. The purpose of this communication is to propose and implement a method which is based on the ASF [21] introduced by one of us, coupled with the recursion method of Haydock, Heine and Kelly [23]. This method retains the *herglotz* properties of the configuration-averaged Green function. The coupling to the recursion method allows effects of quite large clusters to be taken into account. Since the recursion method is intrinsically multisite, off-diagonal disorder and the multisite nature of the LMTOs is not a problem. We shall demonstrate that the use of local point group symmetries of the underlying lattice and the larger symmetries in the full augmented space arising out of the homogeneity of the disorder allows us to work on an irreducible subspace of the augmented space with vastly reduced rank and makes the method tractable even on small desktop workstations.

The paper is organized as follows: in section 2 we briefly review the TB-LMTO method required for the purpose of augmented recursion. In section 3 we discuss the real-space recursion for calculating the Green function, with an emphasis on the symmetry properties which can be exploited to reduce the workload of computation. In section 4 we briefly discuss the augmented-space theorem for the calculation of configuration averages of any function of random variables. Section 5 is devoted to the detailed discussion of the augmented-space recursion method of calculating the configuration-averaged Green function. In section 6 we discuss our results for AgPd, CuZn and FeTi alloys. Conclusions and additional comments regarding the further refinement of our method are given in section 7.

2. Electronic structure calculations with the tight-binding LMTO method

In the LMTO method, an energy-independent basis set $\chi_{RL}(r_R)$ is derived from the energy-dependent partial waves in the form of the muffin-tin orbitals (MTOs). The set is constructed in such a way that it has the following characteristics: (a) it is appropriate to the one-electron effective potential $V(r)$ of the solid; (b) it is a minimal basis set; and (c) it is continuous and singly differentiable over all space. In this section we will restrict ourselves to the most tight-binding representation of the LMTO, resulting in a sparse Hamiltonian, required for the purpose of augmented-space recursion.

As a first step in the LMTO method, the space is partitioned into two regions: the muffin-tin spheres centred at various atomic (if necessary, also interstitial) sites R; and the interstitial region. In the atomic-sphere approximation (ASA) the touching muffin-tin spheres are substituted for with overlapping Wigner–Seitz spheres, thereby dispensing with the interstitial component. It has been argued that if the overlap between the Wigner–Seitz spheres is less than 30% then the ASA is a good approximation and gives reliable results [24].

In the most tight-binding representation, a LMTO basis orbital, with the collective angular momenta index $L = (\ell m)$ centred at site R, is given in the ASA by the expression

$$\chi^{\alpha}_{RL}(r_R) = \phi_{RL}(r_R) + \sum_{R'L'} \dot{\phi}^{\alpha}_{R'L'} h^{\alpha}_{RL,R'L'} \tag{1}$$

where $r_R = r - R$. The function ϕ_{RL} is the solution of the wave equation inside the sphere of radius S_R at R for some reference energy $E_{\nu RL}$ and is normalized within the sphere. The potential inside the sphere is calculated using the local density functional approximation (LDA). The radial part of the $\dot{\phi}^{\alpha}_{RL}$ is related to the energy derivative of $\phi^{\alpha}_{RL}(r_R)$ at the reference energy

$$\dot{\phi}^{\alpha}_{RL}(r_R) = \dot{\phi}_{RL}(r_R) + \phi_{RL}(r_R) o^{\alpha}_{RL}. \tag{2}$$

The quantity $o^{\alpha}_{RL} = \langle \phi_{RL} | \phi^{\alpha}_{RL} \rangle$ is the overlap. The expansion coefficients h_{α} in equation (1) are given by

$$h^{\alpha}_{RL,R'L'} = (C^{\alpha}_{RL} - E_{\nu RL})\delta_{RR'}\delta_{LL'} + (\Delta^{\alpha}_{RL})^{1/2} S^{\alpha}_{RL,R'L'} (\Delta^{\alpha}_{RL})^{1/2} \tag{3}$$

where C^{α}_{RL} and Δ^{α}_{RL} are the potential parameters obtained from the potential function P^{α} at the reference energy $E_{\nu RL}$. $S^{\alpha}_{RL,R'L'}$ is the screened structure matrix whose elements in the most tight-binding representation are essentially zero beyond the second shell of neighbours in all close-packed structures. The screened structure matrix S^{α} can be obtained from the canonical structure matrix S^{0} via the unitary transformation

$$S^{\alpha} = S^{0}(1 - Q^{\alpha} S^{0})^{-1}. \tag{4}$$

The set of parameters (screening constants) Q^{α} which define the above transformation are unique for all closely packed structures, and yield most localized structure constants with exponential decay rather than the usual power-law behaviour.

There are several features of TB-LMTO orbitals which make them distinct from atomic and atomic-like orbitals used in the ordinary TB calculations. The summation over the composite angular momentum index in equation (1) suggests that the TB-LMTO orbitals do not preserve pure L-character. Furthermore, in equation (1) $\dot{\phi}^{\alpha}_{RL}(r_R)$ and ϕ^{α}_{RL} are truncated outside the Wigner–Seitz sphere and the expansion coefficients vanish beyond the second shell of neighbours in all closed-packed structures, so all TB-LMTO orbitals are short ranged, resulting in a sparse Hamiltonian in this representation. This is ideal for real-space calculations based on the recursion method. The Hamiltonian and the overlap matrices for this basis are given by (with the neglect of small terms)

$$H = h + hoh + (I + ho)E_{\nu}(I + oh) \tag{5}$$

$$o = \langle \chi | \chi \rangle = (I + ho)(I + ho). \tag{6}$$

In equations (5) and (6) the summation indices RL are suppressed for convenience. The matrix o is diagonal in the RL-representation and its value is determined by the logarithmic derivative of the function $\dot{\phi}$ at the sphere boundary. The Löwdin orthonormalized Hamiltonian in the ASA is given by

$$H^{(2)} = E_{\nu} + h - hoh + hohoh - \cdots \tag{7}$$

and the first-order Hamiltonian is given by

$$H^{(1)} = E_{\nu} + h. \tag{8}$$

In equation (7) the parameter o determines the degree of non-orthogonality of the basis. Again o^{-1} has the dimension of energy and provides a measure of the energy window about the reference energy E_{ν} for which the densities of states obtained with $H^{(1)}$ are reliable.

In order to perform a recursion calculation, we have to truncate the series given by equation (7) for computational tractability. This in turn introduces non-orthogonality of the basis, so one has to make a compromise between the two for reliable results. The recursion involves repeated operation on the recursive basis with $H^{(2)}$. Since h is sparse, there is, in principle, no additional difficulty (other than enhanced computational time) in going beyond the first-order Hamiltonian. Recursion with $H^{(1)}$ gives a Green function accurate to first order in $E - E_{\nu}$ [24]. The second term hoh is necessary for systems with wide bands, especially for s–p states. We have used a first-order Hamiltonian in our subsequent calculations.

3. The real-space recursion method

The real-space recursion method provides an efficient algorithm for the calculation of the resolvent $(zI - H)^{-1}$ of a sparse Hamiltonian. In this section we will review the recursion method and demonstrate how the symmetry of the Hamiltonian can be exploited to reduce the workload considerably. The method starts with a given vector, $|u_0\rangle$, and recursively generates a new set of vectors $|u_i\rangle$, which are constructed so as to be mutually orthogonal:

$$H|u_n\rangle = a_n|u_n\rangle + b_{n+1}|u_{n+1}\rangle + b_n|u_{n-1}\rangle \tag{9}$$

$$b_0^2 = \langle u_0|u_0\rangle \qquad a_n = \langle u_n|H|u_n\rangle \qquad b_n^2 = \langle u_n|u_n\rangle / \langle u_{n-1}|u_{n-1}\rangle$$

where the recursion coefficients a_n and b_n are the diagonal and off-diagonal elements of the tridiagonal Hamiltonian matrix in the new representation. The method also yields an explicit continued-fraction form for the diagonal elements of the resolvent (the Green function):

$$\langle u_0|(zI - H)^{-1}|u_0\rangle = \cfrac{b_0^2}{E - a_1 - \cfrac{b_1^2}{E - a_2 - \ldots}}. \tag{10}$$

In practice the continued fraction is evaluated to a finite number of steps. Haydock [25] has mapped the contributions of the continued-fraction coefficients to self-avoiding walks on the underlying space. He has shown that the dominant contribution comes from the walks that wind round the initial starting state. This allows one to work only on the finite part of the Hilbert space: a particularly sized cluster around the initial starting state. The continued fraction is complemented after a finite number of steps N with a suitable terminator. The terminator reflects the asymptotic properties of the continued-fraction expansion of the resolvent accurately. Several terminators are available in the literature and we have chosen to use the terminator of Luchini and Nex [26]. The advantage of such a termination procedure is that the approximate resolvent retains the *herglotz* properties. It preserves the first $2(N - 2)$ moments of the density of states exactly. This represents the effect of a cluster at a distance $N - 2$ from the starting state. It also maintains the correct band widths, band weights and singularity of the band edges. It is worth mentioning that, for a tight-binding Hamiltonian, the recursion method involves a workload proportional to the size of the system—rather than the cubic proportionality of the usual band-structure super-cell methods, where the self-consistency is achieved at one k-point.

The workload of the recursion can be further reduced if one exploits the symmetry of the Hamiltonian. The Hamiltonian described by (7) contains information on both the structure of the underlying lattice and the symmetry of the orbitals. It has been shown by Gallagher (see [27]) that if the starting state of the recursion belongs to an irreducible representation of the Hamiltonian, then the states generated in the process of recursion belong to the same row of the same irreducible representation of the Hamiltonian. Furthermore, recursions with starting states corresponding to different rows of the same irreducible representation are similar, but states belonging to the different irreducible representations or different rows of the same irreducible representation do not mix; so we need to retain only *those* states for the purposes of recursion and yet will achieve the same resolution as we would if we retained all of the states. The recursion is performed only with those states which are not related to one another by the point group symmetry of the underlying lattice. Once these state vectors are identified, the recursion can be performed in the reduced space, modified with weighting factors. Thus in the computation we need far less storage and time because the dimensionality of the matrix H is reduced drastically. In practice, a starting site is chosen. The number of distinct equivalent sites, related to the starting site by the local

point group symmetry, constitutes the weighting of the starting site. As discussed earlier, in the process of recursion, these equivalent sites are not considered, and the calculation is confined only to non-equivalent sites. For example for an s-state Hamiltonian on a lattice with cubic symmetry, all of the non-equivalent sites are confined to a (1/48)th portion of the lattice. Inclusion of p orbitals introduces preferred x-, y- or z-directions and breaks the symmetry among the x-, y- and z-axes. Thus the point group symmetry operations which involve interchange among x-, y- and z-coordinates are prohibited. Hence the irreducible part of the lattice, instead of being (1/48)th of the lattice, now becomes (1/8)th. If to each site R we attach weight W_R, which is given by the number of basis states equivalent to $|R\rangle$, then the whole process can be summarized as follows. In the new TB-LMTO reduced basis we have

$$\langle R, L|H|R, L\rangle = C^{\alpha}_{R,L} \tag{11}$$

$$\langle R', L'|H|R, L\rangle = \sqrt{(W_R/W_{R'})}(\Delta^{\alpha}_{R'L'})^{1/2} S^{\alpha}_{R',L',R,L}(\Delta^{\alpha}_{R,L})^{1/2}\beta_R(L, L') \tag{12}$$

where R and R' both belong to the irreducible part of the lattice. $\beta_R(L, L')$ is a factor which can be either 0 or 1, depending on whether the position occupied by the site R is a symmetry position with respect to orbitals L and L' or not. This fact can be made more transparent in the following way: the structure matrix element connecting two orbitals occupying the two different sites is given by the two-centre Slater–Koster integrals. Apart from a factor made up of π- and σ-integrals the Slater–Koster integral contains a factor made up of direction cosines of the vector joining the two basis states that the matrix element is connecting. It reflects the symmetry property of the overlapping orbitals. Now for the different equivalent sites connected to a given site, this direction cosine has different signs. In the effective irreducible basis, which is a linear combination of the old basis states, a particular linear combination may give rise to a zero Hamiltonian matrix element. We shall call these positions, where such zero matrix elements occur, the symmetry positions with respect to orbitals L and L'. The representation of the Hamiltonian in terms of the irreducible basis sets reduces the rank of the Hamiltonian matrix. The workload of the recursion reduces drastically. Such a reduction is absolutely necessary for the purpose of augmented-space recursion to be discussed in the following sections.

4. Augmented-space formalism

The augmented-space formalism enables one to deal with the problem of averaging over disorder configurations. The formalism puts configuration averaging on the same footing as quantum mechanical averaging by augmenting the Hilbert space spanned by the wavefunctions with a disorder or configuration space spanned by the different realizations of the random Hamiltonian. The method of configuration averaging by the augmented-space theorem has been discussed earlier [21], and we shall restrict ourselves just to the salient features of the method.

Let us suppose that the Hamiltonian describing a system is characterized by a set of independent random variables $\{x_i\}$. The probability density of $\{x_i\}$ is assumed to have finite moments to all orders so that we may write

$$p(x_i) = -\frac{1}{\pi}\mathrm{Im}\langle f_0^i|((x_i + \mathrm{i}0)I - M^{(i)})^{-1}|f_0^i\rangle \tag{13}$$

where $M^{(i)}$ is an operator on the space ϕ_0^i of rank N, spanned by the N possible configurations of x_i; and $|f_0^i\rangle$ is the configuration *ground state*. A suitable choice of the

basis is one that makes M^i tridiagonal. This tridiagonal representation may be immediately obtained by looking at the continued-fraction expansion for $p(x_i)$:

$$p(x_i) = -\frac{1}{\pi}\mathrm{Im}\frac{1}{x_i - a_1 - b_1^2 \ldots}. \tag{14}$$

Since $p(x_i) > 0$ and has finite moments to all orders, it always has a convergent continued-fraction expansion with real coefficients $\{a_n, b_n\}$. The representation of $M^{(i)}$ has a_i down the diagonal and b_i in the off-diagonal positions. For a random binary alloy A_xB_{1-x}, $p(n_i)$ may be written as

$$p_i(n_i) = x\,\delta(n_i - 1) + (1 - x)\,\delta(n_i) \tag{15}$$

where

$$n_i = \begin{cases} 1 & \text{for } i = \mathrm{A} \\ 0 & \text{for } i = \mathrm{B}. \end{cases}$$

It immediately follows then that $p_i(n_i)$ satisfies the required conditions, namely

$$\int p_i(n_i) n_i^m \, \mathrm{d}n_i = \text{finite}$$

for all m and

$$p_i(n_i) \geqslant 0.$$

For this $p_i(n_i)$, $M^{(i)}$ is a tridiagonal matrix in a space ϕ_i of rank 2 spanned by $|f_0^i\rangle$ and $|f_1^i\rangle$ with a representation

$$M^{(i)} = \begin{pmatrix} x & \sqrt{x(1-x)} \\ \sqrt{x(1-x)} & (1-x) \end{pmatrix}$$

in this basis.

The formalism now states that the configuration average over any function $H\{x_i\}$ may be written as

$$\int P(\{x_i\}) H\{x_i\} \, \mathrm{d}\{x_i\} = \langle f | \tilde{H} | f \rangle \tag{16}$$

where $\tilde{H}$ is the same functional operator of $\{M^{(i)}\}$ as H was of $\{x_i\}$, and

$$|f\rangle = \Pi^{\otimes} |f_0^i\rangle$$

is the configuration *ground state*. Configuration averaging has been reduced to the problem of finding the *ground-state* matrix element in the augmented space—an idea familiar in quantum mechanical averaging.

5. Augmented-space recursion

It is clear from the discussion in the preceding two sections that, for a system described by a disordered Hamiltonian, the recursion method defined on the augmented space enables one to calculate the configuration-averaged Green function directly. The advantage of the method is that it does not involve a single-site approximation or the solution of any self-consistent equation (which would be required in the CPA or its generalizations). Furthermore, one can treat both diagonal and off-diagonal disorder on an equal footing. In spite of its immense potential the method could not be used for practical calculations because of the large dimension of the augmented space: $N \times 2^N$ for a system with N sites and

disorder characterized by a binary probability distribution. However, in analogy to real-space symmetry, if we exploit the symmetry of the augmented space which arises due to the homogeneity of the disorder, then the rank of the augmented space is reduced and the augmented-space recursion becomes tractable.

The starting point for the augmented-space recursion is the most localized sparse tight-binding Hamiltonian derived systematically from the LMTO-ASA theory and generalized to substitutionally disordered random binary alloys:

$$H^{\alpha}_{RL,R'L'} = \hat{C}_{RL}\delta_{RR'}\delta_{LL'} + \hat{\Delta}_{RL}S^{\alpha}_{RL,R'L'}\hat{\Delta}_{R'L'} \tag{17}$$

$$\hat{C}_{RL} = C^{A}_{RL}n_R + C^{B}_{RL}(1-n_R) \tag{18}$$

$$\hat{\Delta}_{RL} = \Delta^{A}_{RL}n_R + \Delta^{B}_{RL}(1-n_R). \tag{19}$$

Here R denotes the lattice sites and $L = (\ell m)$ are the orbital indices (for transition metal $\ell < 2$). C^{A}_{RL}, C^{B}_{RL} and Δ^{A}_{RL}, Δ^{B}_{RL} are the potential parameters of the constituents A and B of the alloy. n_R are the local site occupation variables which randomly take values 1 and 0 according to whether the site is occupied by an A atom or not. From the discussion in section 4, it is clear that the representation of the Hamiltonian in the augmented space $\tilde{H}$ consists in replacing the local site occupation variables $\{n_R\}$ by $\{M^R\}$, and is given by

$$\tilde{H} = \sum_{RL}\left(C^{B}_{RL}\tilde{I} + \delta C_{RL}\,\tilde{M}^{R}\right)\otimes a^{\dagger}_{R}a_R + \ldots$$
$$+ \sum_{RL}\sum_{R'L'}\left(\Delta^{B}_{RL}\tilde{I} + \delta\Delta_{RL}\,\tilde{M}^{R}\right)S^{\alpha}_{RL,R'L'}\left(\Delta^{B}_{R'L'}\tilde{I} + \delta\Delta_{R'L'}\,\tilde{M}^{R'}\right)\otimes a^{\dagger}_{R}a_{R'}$$

where

$$\delta C_{RL} = (C^{A}_{RL} - C^{B}_{RL}) \qquad \delta\Delta_{RL} = (\Delta^{A}_{RL} - \Delta^{B}_{RL}).$$

Other parameters have their usual meaning and $\tilde{I}$ is the identity operator defined in the augmented space. $\tilde{M}^R$ in the second-quantized notation is given by

$$\tilde{M}^{R} = xb^{\dagger}_{R0}b_{R0} + (1-x)b^{\dagger}_{R0}b_{R0} + \sqrt{x(1-x)}\left(b^{\dagger}_{R0}b_{R1} + b^{\dagger}_{R1}b_{R0}\right). \tag{20}$$

$(b^{\dagger}_{R0}, b_{R0})$ and $(b^{\dagger}_{R1}, b_{R1})$ are the creation and annihilation operators in the augmented space, where each site is characterized by two states (0, 1), which may be identified with the up and down states of an Ising system. The configuration states are stored extremely efficiently in bits of words and the algebra of the Hamiltonian in the configuration space mirrors the multispin coding techniques used in numerical work on the Ising model.

The Hamiltonian is now an operator in a much enlarged space

$$\Phi = H \otimes \Pi^{\otimes}\phi^{R}$$

(the augmented space), where H is the *real space* spanned by the countable basis set $\{|R\rangle\}$. The enlarged Hamiltonian does not involve any random variables but incorporates within itself the full information on the random occupation variables. If we substitute equation (22) for M^R, then with the aid of a little algebra we can show that the augmented-space Hamiltonian contains operators of the following types as discussed in [28].

(a) $a^{\dagger}_{R}a_{R'}$ with $R = R'$ and $R \neq R'$ terms. The operators acting on a vector in the augmented space change only the real-space label, but keep the configuration part unchanged.

(b) $a^{\dagger}_{R}a_{R'}b^{\dagger}_{k\lambda}b_{k\mu}$ with $R = R'$ and $R \neq R'$ terms. k is R or R', while λ and μ may only take the values 0 and 1. These operators acting on an augmented-space vector may change

the real-space label (if $R \neq R'$). In addition, they may also change the configuration at the site R or R' (if $\lambda \neq \mu$). This resembles a single-spin-flip Ising operator in configuration space.

(c) $a_R^\dagger a_{R'} b_{R\lambda}^\dagger b_{R\mu} b_{R'\nu}^\dagger b_{R'\xi}$ with λ, μ, ν, ξ taking the values 0 and 1. The operators may change the real-space label (if $R \neq R'$), as well as the configuration either at R or R' or both. This resembles a double-spin-flip Ising operator in the configuration space.

A basis $|m\rangle$ in the Hilbert space H is represented by a column vector C_m with zeros everywhere except at the mth position. The inner products are defined as

$$\langle m| \odot |n\rangle = C_m^{\mathrm{T}} C_n \qquad a_m^\dagger a_n C_p = \delta_{np} C_m.$$

A member of the basis in $\Pi^{\otimes}\phi_R$ has the form $|f_{\lambda_1}^1 \otimes f_{\lambda_2}^2 \otimes \cdots\rangle$ where each λ_i may be either 0 or 1. We may represent this basis by a collection of binary words (strings of 0s and 1s). In the usual terminology of the ASF the number of 1s defines the cardinality of the basis and the sequence of positions at which we have 1s, $\{S_C\}$, is called the cardinality sequence and labels the basis. Thus a binary sequence $B[C, \{S_C\}]$ is a representation of the member of the basis in the configuration space. The dot product between the basis members is then

$$B[C, \{S_C\}] \odot B[C', \{S_{C'}\}] = \delta_{CC'} \delta_{\{S_C S_{C'}\}}.$$

A careful examination of the operations (a)–(c) defined on the configuration space reveals that these operations change the cardinality and the cardinality sequence. Since the operations are defined on the bits of words, one can easily employ the logical functions in a computer to define these operations.

As mentioned earlier, symmetry considerations arising from the homogeneity of the disorder may be employed to reduce the rank of the effective Hamiltonian in the augmented space. The basic step in the symmetry procedure is to identify a set of non-equivalent vectors and their weights. This can be achieved in the following way. Since the augmented space is a direct product of the real space and the configuration space—which are disjoint—symmetry operations on either of them apply independently of each other. For example, if a site is occupied by an A atom, then all the Z configurations in which $Z-1$ of its neighbours are occupied by A atoms and one is occupied by a B atom are equivalent. In practice a site in the augmented space is chosen as $|R, \{C, [S_C]\}\rangle$. All of the equivalent sites are obtained by the point group operation $\Re$ on the site in question:

$$|R', [C', \{S_{C'}\}]\rangle = \Re |R, [C, \{S_C\}]\rangle = |\Re R, \Re [C, \{S_C\}]\rangle.$$

The number of distinct sites obtained in this way is the weighting of the site in question. As in the real-space recursion only the non-equivalent (NE) sites obtained in this way are retained for the purpose of recursion. Incorporating both the symmetry of the lattice and the orbitals, the representation of the Hamiltonian matrix element is given by

$$\langle RL, [C, \{S_C\}]| \tilde{H} |RL, [C, \{S_C\}]\rangle = [\xi_R \bar{C}_L + (1 - \xi_R)\tilde{C}_L] \tag{21}$$

where

$$I \equiv |R, L\,[C, \{S_C\}]\rangle \in NE$$

$$\xi_R = 1 \qquad R \in S_C$$

$$\xi_R = 0 \qquad R \notin S_C$$

$$\bar{C}_{RL} = x_A C^A + (1 - x_A) C^B$$

$$\tilde{C}_{RL} = (1 - x_A) C^A + x_A C^B.$$

The off-diagonal terms are

$$\begin{aligned}
&\langle R'L', [C', \{S_{C'}\}]|\tilde{H}|RL, [C, \{S_C\}]\rangle \\
&\qquad = \sqrt{W_I/W_J}[\xi_R\xi_{R'}\bar{\Delta}^{1/2}S_{RR'}\bar{\Delta}^{1/2} + \cdots \\
&\qquad\quad +\xi_R(1-\xi_{R'})\bar{\Delta}^{1/2}S_{RR'}\tilde{\Delta}^{1/2} + (1-\xi_R)\xi_{R'}\tilde{\Delta}^{1/2}S_{RR'}\bar{\Delta}^{1/2} + \cdots \\
&\qquad\quad +(1-\xi_R)(1-\xi_{R'})\tilde{\Delta}^{1/2}S_{RR'}\tilde{\Delta}^{1/2}]\beta_I(L, L')\delta_{[C,\{S_C\}],[C'\{S_{C'}\}]} + \cdots \\
&\qquad\quad +\sqrt{W_I/W_J}[\xi_R\bar{\Delta}^{1/2}S_{RR'}(\delta\Delta)^{1/2} + \cdots \\
&\qquad\quad +(1-\xi_R)\tilde{\Delta}^{1/2}S_{RR'}(\delta\Delta)^{1/2}]\beta_I(L, L')\delta_{[C,\{S_C\}],[C'+1,\{S_{C'+1}\}]} + \cdots \\
&\qquad\quad +\sqrt{W_I/W_J}[(\delta\Delta)^{1/2}S_{RR'}(\delta\Delta)^{1/2}]\beta_I(L, L')\delta_{[C,\{S_C\}],[C'+2,\{S_{C'+2}\}]}
\end{aligned}$$

$$\bar{\Delta}_{RL} = x_A\Delta^A + (1-x_A)\Delta^B$$

$$\tilde{\Delta}_{RL} = (1-x_A)\Delta^A + x_A\Delta^B$$

$$\delta\Delta = \Delta^A - \Delta^B.$$

The angular momenta indices are suppressed for convenience. We denote by I and J the augmented-space vectors $|RL, [C, \{S_C\}]\rangle$ and $|R'L', [C', \{S_{C'}\}]\rangle$. $\beta(L, L')$ is 0 or 1 depending on whether or not the position I is a symmetric position with respect to the orbitals L, L' in augmented space. Once we have defined the Hamiltonian, and its operation in augmented space, the recursion method on the augmented space gives the configuration-averaged Green function directly. The recursion method for the calculation of the configuration-averaged Green function $\langle G_{RL,RL}(z)\rangle$ is as follows. We first choose the following as the starting state in our recursion:

$$|\chi_i\rangle = |i \otimes L\rangle \otimes |\psi_0\rangle.$$

The recursion coefficients a_n and b_n are generated by

$$H|u_n\rangle = a_n|u_n\rangle + b_{n+1}|u_{n+1}\rangle + b_n|u_{n-1}\rangle$$

$$a_n = \langle\chi_n| \odot \tilde{H}|\chi_n\rangle \qquad b_n = \langle\chi_{n-1}| \odot \tilde{H}|\chi_n\rangle.$$

The continued-fraction coefficients are each generated to a finite numbers of steps and finally appended with a suitable terminator as discussed earlier. The configuration-averaged Green function is related to the density of states by

$$n(E) = -\frac{1}{N\pi}\mathrm{Im}\sum_L\sum_R\langle G_{RL,RL}(E + \mathrm{i}0)\rangle. \tag{22}$$

6. Results and discussion

The formalism developed in the previous section was applied in calculating the total and local densities of states of random binary alloys at various concentrations. We now mention some details concerning the numerical part of the problem. Total-energy density functional calculations were performed for the elements. The Kohn–Sham equations were solved in the local density approximation (LDA) [29]. The LDA was treated within the context of the method of linear muffin-tin orbitals (LMTO) in the atomic-sphere approximation. The computations were performed semi-relativistically using the exchange–correlation potential of von Barth and Hedin [30]. The basis set was composed of $\ell = 0, 1, 2$ orbitals, so the Hamiltonian elements are matrices of order nine. The elemental potential parameters were used to parametrize the alloy Hamiltonian, incorporating the volume derivative correction for changes with the lattice parameter. The flexibility of the choice of the Wigner–Seitz radius

allowed us to take into account the charge self-consistency approximately as emphasized by Kudrnovský and Drchal [5]. For the purpose of augmented-space recursion, a four-shell augmented-space map was generated from a cluster of 400 sites, with interactions up to second-nearest neighbours for the bcc structure and up to nearest neighbours for the most closely packed fcc-based structures. We have calculated the component and total densities of states through the recursion method with eight pairs of recursion coefficients and terminated with the Luchini–Nex terminator [26]. In some typical cases, such as in CuZn with a low concentration of one constituent, where there are distinct impurity bands, the recursion coefficients were calculated in ten steps. For pure elements, since the densities of states have considerable structure, we employed 15 recursion steps. We have shown in our previous communication [31] that this optimum choice reproduces densities of states comparable to those obtained by other methods.

In the present communication we have studied two fcc-based alloy systems: AgPd and Cu-rich CuZn; and two bcc-based alloy systems: FeTi and Zn-rich CuZn. Our results are discussed below.

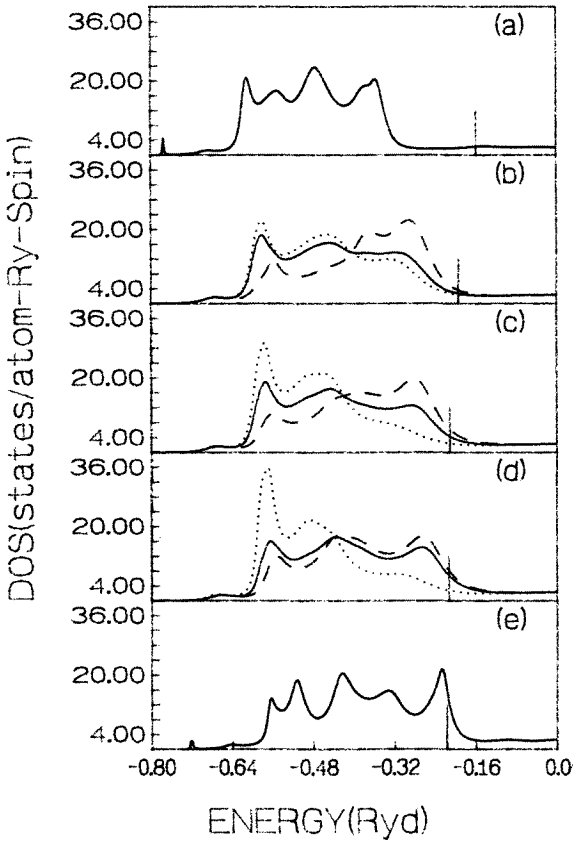

Figure 1. The total (solid) and partial densities of states of Ag (dotted) and Pd (dashed) in Ag_xPd_{1-x} alloys. The concentrations are from top to bottom: $x = 1.0$, 0.75, 0.5, 0.25 and 0. The vertical lines show the position of the Fermi energy.

6.1. AgPd

AgPd is one of the typical alloy systems where the disorder is dominated by the diagonal part of the Hamiltonian. Both constituents have roughly the same d-band widths. Since they belong to the same row of the periodic table, they have very little mismatch in atomic sizes. The alloy remains fcc throughout the concentration regime. Furthermore, since the effect of off-diagonal disorder is weak in this alloy system, the calculations based on the CPA provide good results. Figure 1 shows the total and the component densities of states for the Ag_xPd_{1-x} random systems. Earlier work had looked at the AgPd alloys using the KKR-CPA [32] and the LMTO-CPA [5]. X-ray photoelectron spectra data are available for these alloys [33]. The spectra show a distinct Pd-based impurity peak at around 0.14 Ryd below the Fermi level for low concentrations of Pd and a distinct Ag-based impurity peak at around 0.4 Ryd below the Fermi level for low concentrations of Ag. If we compare our results with figure 3 for the LMTO-CPA in [5] we note that, for all the concentrations quoted, there is close agreement both as regards the dominant peak positions and as regards the general shape of the density of states. Comparison with the KKR-CPA results shows that though the peak positions match reasonably well with ours, the KKR-CPA impurity peaks are much better resolved from the host density of states. The same trend is seen in the experimental results. This comparison indicates that the poor resolution of the impurity peaks is probably not a consequence of the CPA configuration-averaging procedure. It probably arises from the approximations involved in the TB-LMTO method. For AgPd, where the Wigner–Seitz radii of the two constituents are almost the same, we expect the KKR method to be the more accurate band-structure scheme. Table 1 compares the impurity peak positions for the various methods to illustrate our point.

Table 1. Impurity peak positions in Ryd, relative to the Fermi level, for various Ag concentrations in AgPd alloys, obtained by various methods.

KKR-CPA	LMTO-CPA	LMTO-ASR	Experiment
80%	75%	75%	75%
0.139	0.13	0.13	0.147
20%	25%	25%	25%
0.42	0.38	0.34	0.40

6.2. CuZn

CuZn is an important alloy system with both diagonal and off-diagonal disorder. Furthermore, since the centres of the Cu d band and Zn d band are well apart, in the low-concentration limits of Cu and Zn we have impurity bands. It is well known that mean-field theories like the CPA theory do not reproduce the fine structure observed in the impurity bands. Dean [34] first demonstrated the existence of such structure by computer simulation experiments. Careful analysis identified these structures as arising from resonant scattering from clusters of different sizes and shapes immersed in the infinite matrix. The dominant contribution comes from the pair cluster with the characteristic bonding and antibonding peaks. The CPA, being a single-site approximation, cannot reproduce these structures. This analysis was carried out in detail in an earlier paper [35]. This system provides a testing ground of our methodology which takes us beyond the CPA.

If we carefully examine the phase diagram of Cu_xZn_{1-x} alloy, we find that it is

dominated by several ordered structures along with both fcc (α) and bcc (β) solid solutions. In our calculation we will assume fcc (α) solid solutions for $x > 0.5$ and bcc (β) solid solutions for $x < 0.5$. For $x = 0.5$ one has the well known β-brass, for $x = 0$ the hcp Zn and for $x = 1.0$ the fcc Cu structure.

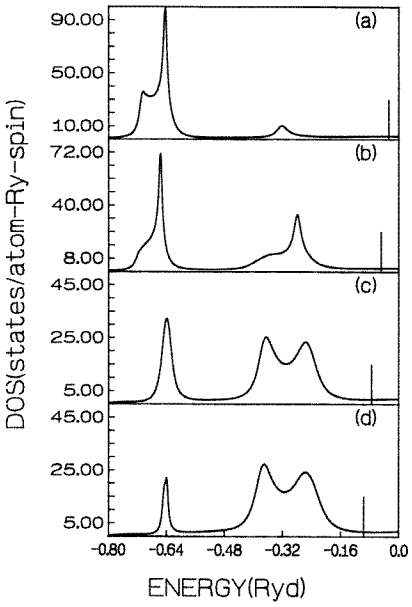

Figure 2. The total density of states for Cu_xZn_{1-x} alloys: (a) bcc with $x = 0.1$; (b) bcc with $x = 0.5$; (c) fcc with $x = 0.75$; and (d) fcc with $x = 0.9$.

Figure 2 shows the total and the local densities of states for the Cu_xZn_{1-x} alloy for $x > 0.5$ where the lattice structure is taken as fcc and for $x < 0.5$ with the alloy assumed to be in a bcc phase. We find that the large differences among the d-band centres of the constituents and the differences among their widths get reflected in the densities of states. We notice that the density of states in the bcc phase has similar features to that for the fcc structure.

Figure 3(a) shows the Cu_xZn_{1-x} alloy with $x = 0.9$. The dotted curve was obtained by a four-step recursion, and invoking a moment argument one can compare this result with the characteristic featureless CPA density of states. The solid one was obtained by a ten-step augmented-space recursion. In order to look slightly deeper into the origins of the structures in the impurity band, we have shown in figure 3(b) the density of states of a single Zn atom immersed in the alloy together with the single-atom d-state energy level (-0.625 Ryd). In figure 3(c) we have shown a cluster of 13 zinc atoms (one central and its twelve nearest neighbours) immersed in the alloy medium. The single immersed impurity shows a featureless band formed from the single-atom impurity level, shifted slightly due to crystal-field effects and broadened due to its immersion in the alloy. For the embedded cluster the impurity band already shows the two-peaked structure apparent in figure 3(a), reminiscent of zinc–zinc bonding and antibonding states immersed in an alloy medium. In figure 3 (right-hand panel) we have plotted the density of states for Cu_xZn_{1-x} alloy with $x = 0.1$ and we observe the same cluster effects at the Cu site.

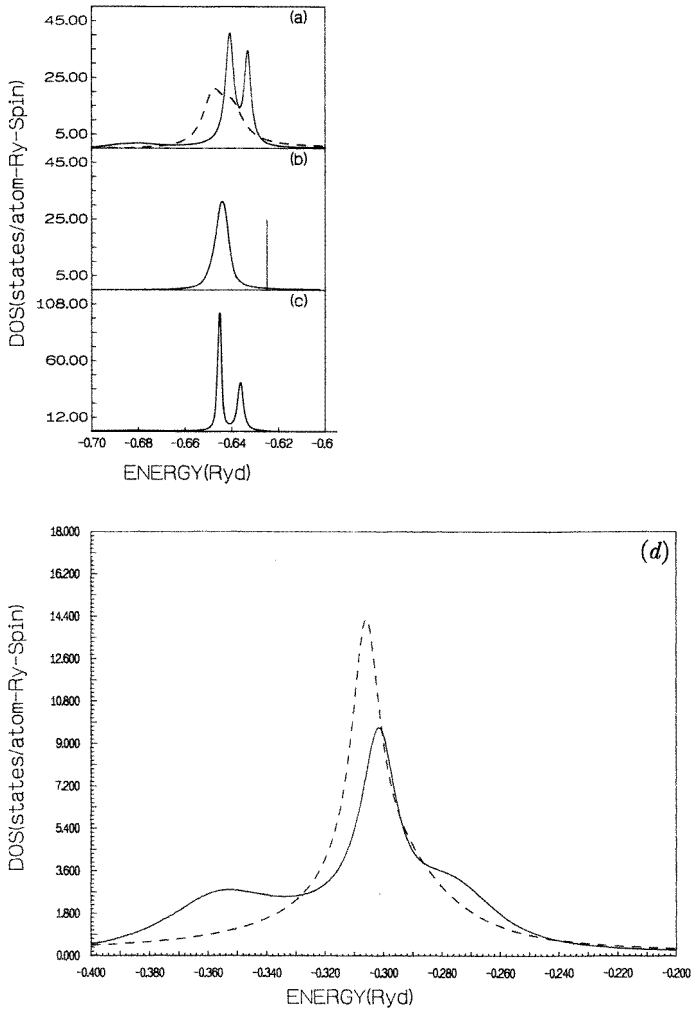

Figure 3. (a) The partial density of states at the Cu site in bcc Cu_xZn_{1-x} with $x = 0.9$ (dotted) from the CPA (full) ASF calculation with ten recursion steps. (b) The partial density of states of a single Zn atom immersed in the alloy medium. The arrow marks the d-state energy level of a single zinc atom. (c) The partial density of states at the central zinc site of a nearest-neighbour zinc cluster (13 atoms) immersed in the alloy medium. Right-hand panel: the partial density of states at the Zn site in fcc Cu_xZn_{1-x} with $x = 0.9$ (dotted) from the CPA (full) ASF calculation with ten recursion steps.

6.3. FeTi

TiFe alloy exhibits strong diagonal disorder and non-negligible off-diagonal disorder, and the constituent atoms have very different sizes. Such differences in constituent radii lead to local lattice distortion effects in this alloy system. We shall take up this problem in a later communication. The bcc disordered phase exists in Ti-rich alloys with concentration of Ti $\geqslant 0.77$, and for $x = 0.5$ the ordered CsCl phase is known to exist and is found to be very stable. We have calculated the density of states of disordered TiFe by augmented-space recursion in the bcc phase at various concentrations. Theoretical band-structure calculations

for TiFe are available for both the TB-LMTO-CPA [5] and the KKR-CPA [36].

In order to see the effect of disorder on the density of states of TiFe we have shown in figure 4 (top panel) the density of states of ordered 50–50 TiFe in the CsCl structure obtained by the LMTO method. We find that the d-band complex due to Fe and Ti breaks into two gaps, separated by a deep minima where the Fermi energy E_F falls. The lower states are predominantly Fe d states while the states above minima are mostly Ti d states. Furthermore, the states lying below the minimum may be interpreted as Fe–Ti bonding states while those above the minimum are the antibonding states. Since the bonding states are filled, the ordered system is energetically favoured. If we compare this with the KKR-CPA calculations, we find that there is marked broadening of all the structures which is a clear indication of strong-disorder scattering. The most interesting effect is the suppression of the gap at $E = E_F$. This suggests that many filled (unfilled) levels have been raised (lowered) in energy, so the energy of the disordered phase is higher. In figure 4 (bottom panel) we have presented our ASR calculations for Ti_xFe_{1-x} at various concentrations (from top to bottom $x = 1.0, 0.5, 0.2, 0.0$). We find that the gap in the density of states disappears due to disorder scattering, analogously to the KKR-CPA result. A similar feature is observed in TB-LMTO-CPA calculations.

Our preliminary calculation excluding lattice relaxation effects and proper treatment of the charge-transfer effect shows that the results compare satisfactorily with earlier calculations, proving the applicability of the methodology to different alloy systems.

7. Conclusions

The calculation scheme developed in this work is based on three methodologies: (i) the TB-LMTO method for the description of the Hamiltonian; (ii) the augmented-space theorem for the configuration averaging; and (iii) the recursion method applied to augmented space to obtain the configuration-averaged Green function.

The TB-LMTO Hamiltonian is free from fitted parameters. The potential parameters entering into the Hamiltonian are derived self-consistently. However, it carries with it the approximations involved in the linearization which leads to the LMTO. The recursion method requires the use of a sparse Hamiltonian. We have to base our method on a less accurate Hamiltonian (with a truncation of the infinite series (7)) than the Hamiltonian in the so-called γ-representation used in the CPA calculations. However, Nowak *et al* [16] have shown that the calculations for the density of states converge rapidly as we take more terms in the series in equation (7).

The configuration-averaging scheme is based on the augmented-space theorem, which is formally exact. The use of the recursion technique with suitable terminators applied to the augmented space, so constructed, ensures that the TB-LMTO-ASR Green functions retain the essential *herglotz* analytic properties. In addition, the method can take into account cluster effects, off-diagonal effects arising due to disorder in the structure matrix, and correlated disorder [37].

The recursion method carries errors which are dependent on the finite cluster size and the nature of terminators used, both of which cause the electrons to experience a medium that deviates from the intended structures away from the central sites [15]. The choice of proper terminators partially solves the problem and one should choose larger clusters with greater numbers of recursion steps for more accuracy. The recursion method is a well established procedure that has been proven to produce a very accurate density of states for d bands for 8 to 15 recursion steps (that is, it yields 16 to 30 moments of the density of states exactly).

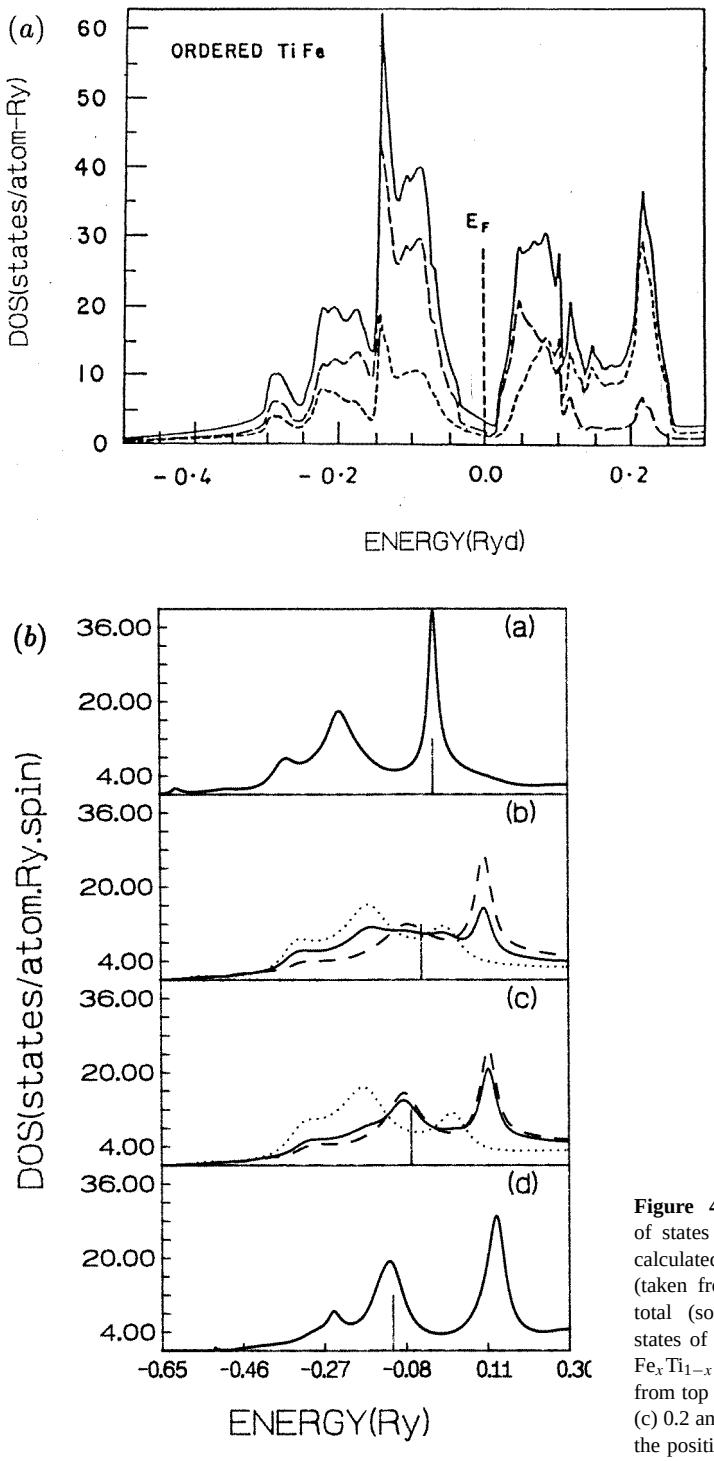

Figure 4. Top panel: the density of states for ordered 50–50 FeTi alloy calculated by the TB-LMTO method (taken from [36]). Bottom panel: the total (solid) and partial densities of states of Ti (dotted) and Fe (dashed) in Fe_xTi_{1-x} alloys. The concentrations are from top to bottom: $x =$ (a) 1.0, (b) 0.5, (c) 0.2 and (d) 0. The vertical lines show the position of the Fermi energy.

In summary, we should like to propose the TB-LMTO-ASR technique as a simple, accurate and computationally efficient method for the first-principles calculation of the electronic structure of disordered solids.

Acknowledgments

We should like to record our thanks to Patricio Vargas for the use of his real-space structure factor program and to G P Das for several fruitful discussions. AM would like to acknowledge the funding from the Department of Science and Technology (project SP/S2/M09/93) and the International Centre for Theoretical Physics (the Network on Metals and Alloys).

References

[1] Pettifor D 1992 *Electron Theory in Alloy Design* ed D Pettifor and A Cottrell (London: The Institute of Materials) p 81
[2] Andersen O K and Jepsen O 1984 *Phys. Rev. Lett.* **53** 2571
[3] Carr R and Parinello M 1985 *Phys. Rev. Lett.* **55** 2471
[4] Methfessel M and Schilfgaarde M 1993 *Int. J. Mod. Phys.* B **7** 262
[5] Kudrnovský J and Drchal V 1990 *Phys. Rev.* B **41** 7515
[6] Kudrnovský J, Bose S K and Andersen O K 1991 *Phys. Rev.* B **43** 4613
[7] Singh P P and Gonis A 1993 *Phys. Rev.* B **48** 1989
[8] Slater J C 1937 *Phys. Rev.* **51** 846
[9] Korringa J 1947 *Physica* **13** 392
Kohn W and Rostocker N 1954 *Phys. Rev.* **94** 1111
[10] Jansen H J F and Freeman A J 1984 *Phys. Rev.* B **30** 561
[11] Andersen O K 1975 *Phys. Rev.* B **12** 3060
[12] See references in
Stocks G M and Winter H 1985 *Electronic Structure of Complex Systems* ed P Phariseau and W M Temmerman (New York: Plenum)
[13] Kumar V, Mookerjee A and Srivastava V K 1982 *J. Phys. C: Solid State Phys.* **15** 1939
[14] Gonis A, Butler W H and Stocks G M 1983 *Phys. Rev. Lett.* **50** 1482
[15] Bose S K, Kudrnovský J, Jepsen O and Andersen O K 1992 *Phys. Rev.* B **45** 8272
[16] Nowak H J, Andersen O K, Fujiwara T, Jepsen O and Vargas P 1991 *Phys. Rev.* B **44** 3577
[17] Gonis A, Stocks G M, Butler W H and Winter H 1984 *Phys. Rev.* B **29** 555
[18] Tsukada M 1972 *J. Phys. Soc. Japan* **32** 1475
[19] Gray L J and Kaplan T 1976 *J. Phys. C: Solid State Phys.* **9** L303, L483; 1976 *Phys. Rev.* B **14** 3462; 1977 *Phys. Rev.* B **15** 3260, 6005
[20] Mookerjee A 1987 *J. Phys. C: Solid State Phys.* **17** 1511
[21] Mookerjee A 1973 *J. Phys. C: Solid State Phys.* **6** 1340
[22] Rajput S S, Razee S S A, Prasad R and Mookerjee A 1990 *J. Phys.: Condens. Matter.* **2** 2653; 1990 *Phys. Rev.* B **42** 9391
[23] Haydock R, Heine V and Kelly M J 1972 *J. Phys. C: Solid State Phys.* **5** 2845
[24] Andersen O K, Jepsen O and Glötzel D 1985 *Highlights of Condensed Matter Theory* ed F Bassani, F Fumi and M P Tosi (Amsterdam: North-Holland) p 59
[25] Haydock H 1972 *PhD Thesis* University of Cambridge
[26] Luchini M U and Nex C M M 1987 *J. Phys. C: Solid State Phys.* **20** 3125
[27] Haydock R 1980 *Solid State Physics* vol 35 (New York: Academic)
Gallagher J 1978 *PhD Thesis* University of Cambridge
[28] Datta A and Mookerjee A 1992 *Int. J. Mod. Phys.* B **6** 3295
[29] Kohn W and Sham L J 1965 *Phys. Rev.* **140** A1133
[30] von Barth U and Hedin L 1972 *J. Phys. C: Solid State Phys.* **5** 1629
[31] Saha T, Dasgupta I and Mookerjee A 1994 *J. Phys.: Condens. Matter* **6** L245
[32] Winter H and Stocks G M 1983 *Phys. Rev.* B **27** 882
[33] Hüfner S, Wertheim G K and Wernick J H 1973 *Phys. Rev.* B **8** 4511

[34] Dean P 1960 *Proc. R. Soc.* A **254** 507
[35] Kumar V, Mookerjee A and Srivastava V K 1982 *J. Phys. C: Solid State Phys.* **15** 1939
[36] Da Silva E Z, Strange P, Temmerman W M and Gyorffy B 1987 *Phys. Rev.* B **36** 3015
[37] Razee S S A and Prasad R 1993 *Phys. Rev.* B **48** 1349, 1361
Datta A, Thakur P K and Mookerjee A 1993 *Phys. Rev.* B **48** 8567
Mookerjee A and Prasad R 1993 *Phys. Rev.* B **48** 17 724